iScience

Article

Design and *in-situ* biomimetic fabrication of a high-density strain sensor array for parachute canopy fabric

Graphical abstract

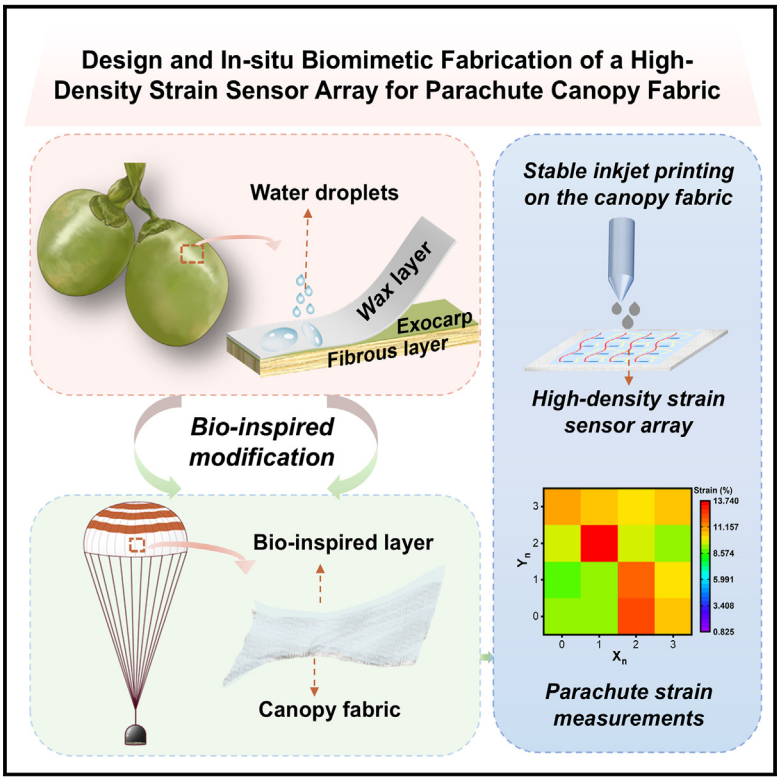

Highlights

- A biomimetic method for modifying parachute fabric for stable inkjet printing is provided
- A high-density strain sensor array on the parachute canopy fabric is fully printed
- The measurement of non-uniform strains in the parachute canopy fabric is realized

Authors

Hui Li, Jiangang He, Chunzu Liang, ..., Dengbao Xiao, He Jia, Wei Rong

Correspondence

xiaodengbao@bit.edu.cn (D.X.), chinajiah@163.com (H.J.)

In brief

Sensor; Polymers; Surface science

Li et al., 2025, iScience *28*, 111794
February 21, 2025
https://doi.org/10.1016/j.isci.2025.111794

CellPress

iScience

CellPress
OPEN ACCESS

Article

Design and *in-situ* biomimetic fabrication of a high-density strain sensor array for parachute canopy fabric

Hui Li,[1,5] Jiangang He,[2,5] Chunzu Liang,[3] Fengjiao Bin,[1] Xu Li,[1] Xianda Wang,[1] Zihao Wang,[1] Xiangxiao Bu,[1] Dengbao Xiao,[1,6,*] He Jia,[4,*] and Wei Rong[4]

[1]Institute of Advanced Structure Technology, Beijing Institute of Technology, Beijing 100081, China
[2]AVIC Chengdu Aircraft Design & Research Institute, Chengdu 610091, China
[3]Beijing Satellite Manufacturing Factory, Beijing 100086, China
[4]Beijing Institute of Space Mechanics & Electricity, Beijing 100094, China
[5]These authors contributed equally
[6]Lead contact
*Correspondence: xiaodengbao@bit.edu.cn (D.X.), chinajiah@163.com (H.J.)
https://doi.org/10.1016/j.isci.2025.111794

SUMMARY

In-situ monitoring of non-uniform strains in spacecraft parachute canopies is essential to ensure safe landings. Traditional wearable strain sensors struggle to meet high-resolution measurement requirements due to their low density. *In-situ* inkjet printing offers a promising solution for fabricating high-density strain sensor arrays directly on the fabric surface. However, capillary effects in the canopy fabric cause droplet leakage, hindering stable printing. To address this, we drew inspiration from nature, using modified silane to mimic the wax layer of coconut husk for modifying the canopy fabric, which enabled the *in-situ* fabrication of a strain sensor array via inkjet printing. This modification overcame capillary effects and balanced the fabric's wettability, essential for stable printing. Furthermore, a layered printing strategy was designed to increase sensor density to 4 units·cm^{-2}, facilitating high-resolution measurement of non-uniform strains in the canopy. This study offers a feasible approach for developing sensors for large-scale parachute strain measurements.

INTRODUCTION

Parachutes utilize aerodynamic drag to decelerate, ensuring the controlled and stable landing of spacecrafts.[1] The parachute's primary load-bearing components include the canopy and suspension lines. The canopy is constructed from stitched fabric panels rather than a monolithic structure, commonly experiencing non-uniform deformation during working. Additionally, during spacecraft landing, the parachute is subjected to complex environmental factors such as temperature variations, dynamic loads, wind speeds, etc. Poor design of the main canopy fabric structure can cause the tear and destruction of the parachute fabric, leading to hazardous situations. Therefore, monitoring the non-uniform strains in the parachute fabric under operational conditions can enhance our understanding of the mechanisms involved in the deployment, inflation, and descent phases, which is crucial for optimizing the structural design of parachutes.[2–4] Because strains are distributed across the entire parachute fabric, effective monitoring requires large-area measurement rather than discrete-point measurement, necessitating the development of strain sensor arrays. Based on calculations using the fiber distribution on the fabric surface of Chinese spacecraft parachutes, a strain sensor array density of at least 4 units·cm^{-2} is required for high-resolution measurement of the parachute fabric's strains during working. However, existing reports on strain sensor arrays have primarily focused on flexible electronics for monitoring physiological movements, with few strain sensor arrays achieved the density of 4 units·cm^{-2}.[5–8] Their densities cannot meet the requirements for strain sensor arrays used in parachutes. In addition, the limited reports on parachute strain sensors are primarily designed for single-point measurements.[9–12] Therefore, it is important to design strain sensor arrays to meet the density requirements of parachutes.

Fabric-based flexible sensors integrate functional sensing materials such as conductive organic polymers, metallic nanoparticles/nanowires, carbon-based materials, into textile, integrating them as part of the fabric structure.[13–16] They exhibit superior mechanical compliance compared to metal strain gauges and optical fiber sensors, enabling precise strain measurements.[17–20] The fabrication methods of fabric-based sensors include weaving, coating, and so on. Although the weaving method can fabricate sensitive strain sensors, differences in mechanical properties between conductive fibers and fabrics may lead to distinct strain behaviors, potentially resulting in inaccurate strain signals.[21] The coating methods not only increase accuracy but also simplify the construction of high-density strain sensor arrays. Digital inkjet printing, classified as a coating technique, is a mask-free method with high time efficiency and spatial resolution,

ensuring the large-scale and low-cost fabrication.[22] It enables on-demand deposition of functional inks, thereby enabling the efficient and scalable production of high-density strain sensor arrays.[23–25] For water-based conductive ink, it is essential to balance the hydrophilicity and hydrophobicity of the printing substrate.[26,27] A highly hydrophobic substrate may cause ink droplets to roll, hindering stable deposition, while a highly hydrophilic substrate can result in excessive spreading of ink droplets, leading to blurred patterns and edges.[28,29] Thus, achieving proper wettability is a critical prerequisite for high-quality inkjet printing. More importantly, the presence of micro-pores, capillaries, surface defects, and inter-fiber voids within the fibers of parachute fabric often leads to capillary effects during inkjet printing,[30–32] causing ink penetration and blurred patterns. Consequently, overcoming capillary effects and achieving balanced wettability are significant challenges in ensuring continuous high conductivity in printed circuits on fabrics.[33]

Currently, the primary methods for adjusting substrate wettability involve introducing micro-nano structures or modifying the chemical composition of the materials.[34] However, due to their complexity and expensiveness, these methods are not suitable for large-scale parachute fabric. Therefore, it is of great importance to find a cost-effective method that preserves the material's intrinsic mechanical properties while imparting proper wettability to enhance the inkjet printing performance on the substrate. It is well known that the outermost layer of most plants is covered by a dense, colorless, and transparent waxy layer primarily composed of very long-chain fatty acids and their derivatives, including aldehydes, alcohols, alkanes, ketones, esters and triterpenoids. This layer can prevent water loss, rain impact, and pathogen infection, thereby maintaining plant's water balance and promoting healthy growth.[35] Inspired by the waxy layer on the plant surfaces, directly coating a thin, modified layer similar to waxy layer onto the fabric surface may overcome the capillary effects and enable successful inkjet printing.

Here, drawing inspiration from nature, we propose a simple and low-cost fabric modification method that enables direct inkjet printing on the parachute canopy fabric, facilitating the *in-situ* fabrication of a high-density strain sensor array to measure the canopy's non-uniform strains. First, inspired by the waxy layer on coconut shells, we innovatively used lost-cost modified silane (MS) to modify parachute canopy fabric. This method not only overcame the capillary effects in fabrics, but also balanced the wettability of the substrate, enabling stable inkjet printing of water-based inks on the fabric. By utilizing water-based conductive polymers, poly (3,4-ethylenedioxythiophene): poly (styrene sulfonate) (PEDOT:PSS), we successfully fabricated a high-density strain sensor array (4 units·cm^{-2}) through a layered circuit printing strategy. Ultimately, we performed *in-situ* fabrication of a 4 × 4 array of flexible, high-density strain sensors on the canopy fabric. The sensor unit on the canopy fabric exhibited good sensitivity and linearity during measuring strains. What's more, the resulting sensor array was integrated into a custom-built strain monitoring system and experimental results confirmed its effectiveness in high-resolution monitoring the strain distribution of canopy fabric. The proposed design and fabrication of the fabric-based strain sensor array provide a feasible approach for measuring large-scale parachute strains.

RESULTS AND DISCUSSION

FEA for non-uniform strains of the canopy fabric

During the deceleration and landing process of spacecraft, the parachute is in a complex environment. We simply investigated the strain distribution of the parachute fabric under uniaxial tension, biaxial tension, and dislocation by constructing a model of the fabric and performing finite element analysis (FEA). As shown in Figures 1A and 1B, during uniaxial tension, the entire deformation process was supported by the tensioned fabric yarns. Apart from the yarns in tension direction undergoing deformation, yarns in the orthogonal direction remained unaffected. Upon fabric failure, the fabric components lost the weft yarn constraint, rendering them unable to maintain the original woven structure. As shown in Figure 1C, during biaxial tension, the load-bearing structure consisted of weft and warp yarns. The failure process occurred at the intersection area, culminating in the complete failure of the entire connecting structure. As shown in Figure 1D, during dislocation process, the load-bearing structure underwent complex changes, initially comprising the outermost yarns. As displacement increased, various degrees of load appeared across the intersection areas. Ultimately, the failure of the canopy fabric gradually occurred, culminating in a complete rupture. FEA results indicated that the parachute fabric underwent diverse deformation conditions during operation. Therefore, accurate measurement and analysis of the non-uniform strains are crucial for ensuring the optimal design of parachutes and safe landing of spacecrafts.

Bionic surface modification of the canopy fabric

The capillary effects of parachute canopy fabric caused the adsorption and penetration of water-based silver nanoparticle ink into the fabric substrate, often resulting in blurred patterns and discontinuities in printed circuits. The parachute fabric used in this study was woven from nylon-66 fibers. As illustrated in Figure S1, inkjet printing on the unmodified fabric resulted in blurred circuit lines. Therefore, surface modification of the fabric was necessary to eliminate capillary effects and achieve continuous high conductivity in the printed circuits. As shown in Figure S2, experimental results demonstrated that on a highly hydrophobic polydimethylsiloxane (PDMS) surface, conductive ink droplets coalesced, producing discontinuous patterns. In contrast, when the printing substrate was replaced with a hydrophilic polyurethane surface, which offered better interfacial interaction with the conductive ink, the resulting patterns were smooth and uniform. Therefore, the selection of a modified material with proper wettability for water-based ink was crucial for achieving optimal inkjet printing outcomes.

It is well known that numerous plant surfaces in nature are covered with a dense, isolated waxy layer that serves as a physical barrier. This waxy layer prevents external water and pathogens from penetrating the plant's epidermis, reduces internal water loss, and ensures that external water droplets do not infiltrate the plant's internal structure, while not interfering with the normal activities and functions of the leaves.[36,37] This inspired us to modify the canopy fabric substrate for overcoming capillary effects. To further investigate the hydrophilicity and hydrophobicity of the waxy layer, specifically, we selected three fresh plant components for analysis: semiaquilegia adoxoide leaves,

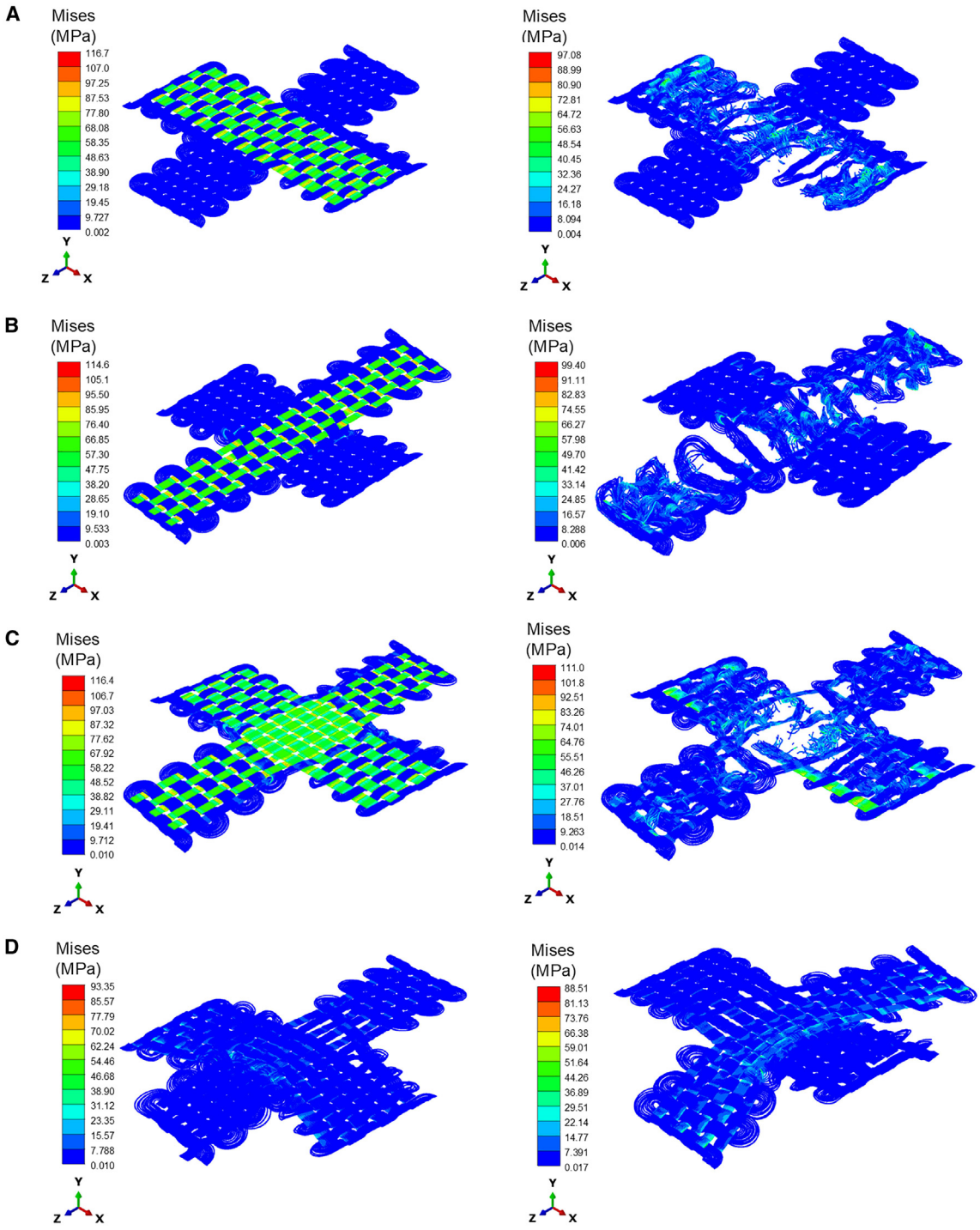

Figure 1. FEA results of the parachute canopy fabric deformed under three conditions

(A and B) FEA results of the parachute canopy fabric under uniaxial tension.

(C) FEA results of the parachute canopy fabric under biaxial tension.

(D) FEA results of the parachute canopy fabric under dislocation.

lagedium sibiricum leaves, and coconut shells. The water contact angles (WCAs) of these samples were measured to evaluate the hydrophobicity or hydrophilicity of their external waxy layers. As shown in Figures 2A and S3, the WCAs for these three plants were 114.924°, 112.223°, and 75.468°, respectively.[38,39] Since water-based ink needed to both overcome capillary effects

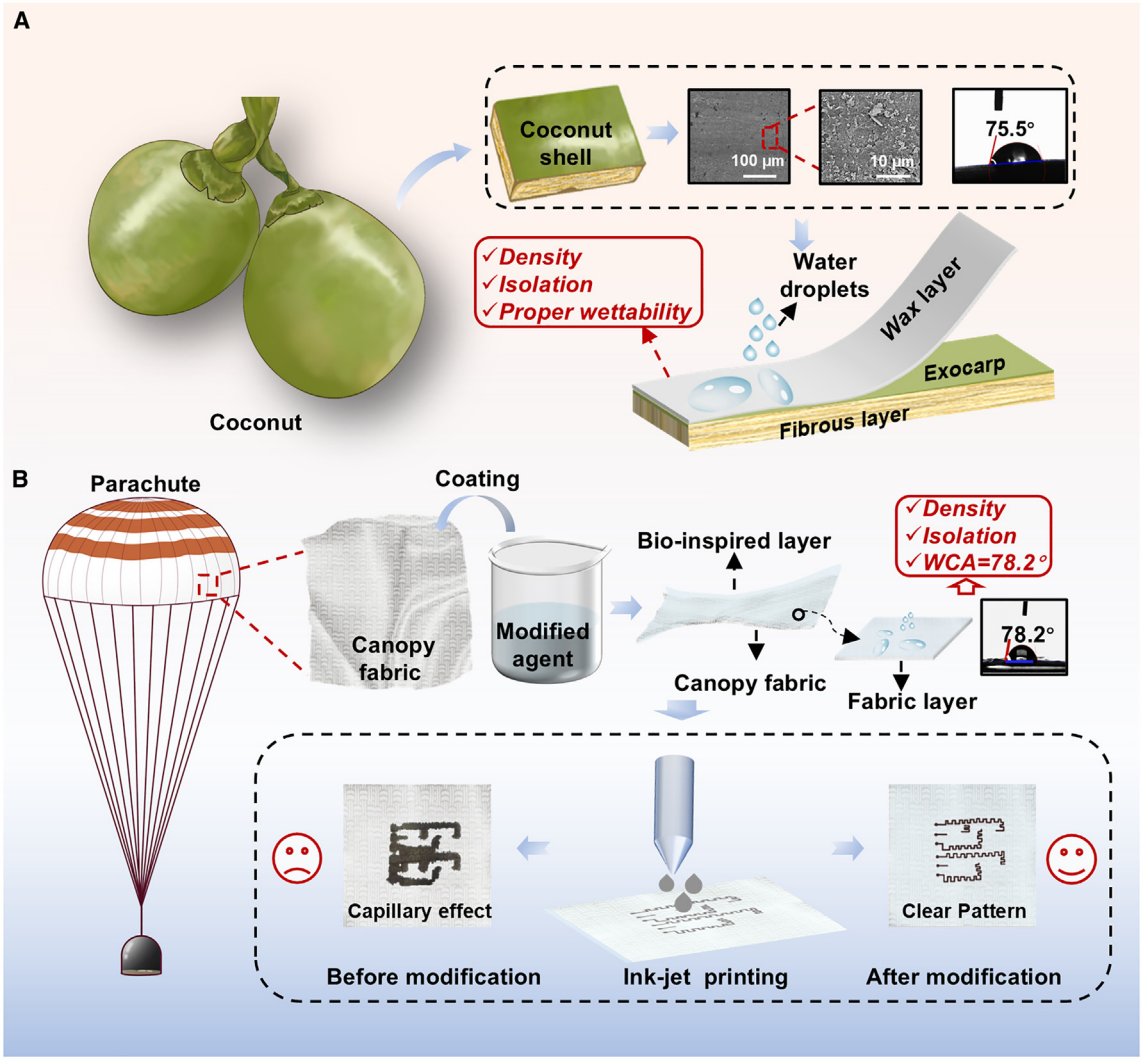

Figure 2. The biomimetic modification of parachute fabric

(A) Schematic diagrams of a coconut and its shell, accompanied by the structure, SEM images, and water contact angle of the waxy layer.

(B) Schematic diagrams of the biomimetically modified parachute fabric for stable inkjet printing.

and spread on the surface to form clear patterns, we inferred that the more hydrophilic properties of the waxy layer on the coconut shell would be suitable for inkjet printing. To clearly see the wax layer, as shown in Figure 2A, coconut shells were characterized using cryoelectron microscopy. The surface waxy layer of the coconut shell was smooth with no obvious microstructures,[40,41] primarily acting as a dense and isolated waxy coating. Inspired by this, as shown in Figure 2B, we imitated this protective layer to overcome capillary effects of parachute fabric and balance the wettability of the fabric for successful inkjet printing. However, direct synthesis of waxy materials was challenging. Therefore, we sought an alternative coating for the parachute fabric that could provide a cost-effective surface modification to overcome capillary effects and achieve the required wettability. First, we used every-day nail polish to modify the fabric. After applying and drying the nail polish on the parachute fabric, we successfully performed inkjet printing using a silver nanoparticle ink solution on the canopy fabric. As shown in Figure S4, the printed silver nanoparticle ink remained stable and did not flake off despite repeated folding and rubbing, demonstrating the feasibility of the surface modification. However, nail polish hardened and became brittle upon drying, which negatively affected the intrinsic mechanical properties of the parachute. To ensure that the mechanical properties of the fabric remained unchanged post-modification, the surface modification material should exhibit a low elastic modulus for good conformality. Moreover, after printing the conductive ink, it needed to be cured and formed at 150°C. Therefore, the surface modification material also should exhibit robust high-temperature resistance.

Through extensive trials, we discovered that MS, a widely used sealant based on end-silane polyether as the fundamental polymer, demonstrated good adhesion to substrates. Moreover, MS

exhibited a low elastic modulus and high-temperature resistance. Therefore, MS was employed as a surface modifier for parachute fabric. As shown in Figure S5, optical microscopy and scanning electron microscopy (SEM) images demonstrated that the original unmodified parachute fabric had noticeable pores among the fibers. After modification with MS, the surface of the parachute fabric appeared smoother, with the pores effectively eliminated. Contact angle measurements showed that the WCAs of the fabric before and after modification were both approximately 78°, indicating minimal change in wettability. However, detailed observations during the testing process showed that when water droplets were dropped on the unmodified fabric, they were quickly absorbed by the fabric within 5 s, resulting in a WCA of 0°. In contrast, when water droplets were dropped on the surface of the modified fabric and observed with a camera over a period of 10 s, the fabric did not exhibit macroscopic absorption of the droplet, and the WCA remained constant. These results indicated that coating with MS effectively eliminated the fabric's capillary effects. What's more, the modifier imparted appropriate wettability to the canopy fabric, ensuring stable inkjet printing patterns with clear edges and good uniformity. Furthermore, we inferred that the mechanism by which the modified surface achieves suitable wettability for inkjet printing could be explained by the concept of contact angle hysteresis,[42] which resulted from the combined repulsive and attractive forces between the inkjet and the surface. This study focuses on the wettability properties of the modified surface, while the underlying mechanism will be explored in greater detail in our future research.

Design and fabrication of the strain sensor unit and array

Design and fabrication of the strain sensor unit

PEDOT:PSS is a classic conductive polymer widely employed in various fields, including flexible electronics,[43] sensors,[44] and organic light-emitting diodes (OLEDs).[45] PEDOT exhibits high conductivity, reaching up to 300 S cm^{-1}, but has poor water solubility. Insulating PSS can stabilize the dispersion of PEDOT and endow PEDOT with water solubility and processing performance. We chose PEDOT:PSS as the conductive ink and employed inkjet printing to fabricate the sensing section of the strain sensor. As shown in Figure 3A, the strain sensor unit consisted of two components: the PEDOT:PSS sensing section and the conductive silver electrode. The sensing section was a rectangular high-resistance area with a size of 2.5 mm × 1 mm, and the conductive silver circuit was low-resistance area with a width of 0.5 mm. When the parachute fabric was subjected to strain, the resistance of the PEDOT sensing section exhibited a corresponding change. The sensitivity of the strain sensor was represented by gauge factor (GF), defined as the ratio of the relative change in electrical signals to the applied strain.[46] The GF of this strain sensor was calculated by the equation below:

$$GF = \frac{\Delta R}{\varepsilon R_0}$$

where R_0 was the original resistance, and ΔR was the relative change of resistance, and ε was the applied strain.

In order to measure and calibrate the electromechanical performance of the sensor unit, we fixed the parachute canopy fabric, which was printed with an ink-jet printed sensor unit, in the clamps of the tensile testing machine. The two ends of the sensor unit were boned with copper wires using conductive silver paste. The fabric was stretched at a speed of 100 mm min^{-1} and resistance changes were measured by using an Inductance, Capacitance, Resistance (LCR) digital bridge. As shown in Figure 3B, the sensor unit showed a GF value of 8.723 and a linearity with a goodness-of-fit R^2 value of 0.9882. Consequently, the stretching tests confirmed that the sensor unit enabled accurate parachute strain measurements, exhibiting both good sensitivity and excellent linearity, thereby demonstrating its suitability for constructing a sensor array.

Design and fabrication of a high-density strain sensor array

The single sensor unit could only measure the strain of discrete point. However, during parachute operation, non-uniform strains were distributed across the entire fabric surface. To accurately monitor the non-uniform strains at various locations across the parachute canopy fabric, it was necessary to design and print a sensor array to ensure large-area conformal coverage. Therefore, a flexible strain sensor array was fabricated by inkjet printing on the parachute canopy based on the single sensing unit. As shown in Figure 3C, in order to simplify the construction layout of conductive circuits and maximize the density of the sensor array, we designed a circuit with shared electrodes and conductors to avoid the complexity of setting up individual sensing units, electrodes, and lead wires.[47] Each column of sensor units shared one side electrode, and the conductive lines were arranged vertically. Each row of sensor units shared the other side electrode, and the conductive lines were arranged horizontally. All silver conductive lines were designed with an S-shaped curve to minimize resistance changes caused by the deformation of silver lines. The endpoints of the horizontal and vertical conductive lines were printed with pads for the connection to the signal acquisition system. This design approach expanded the effective measurement area and facilitated the construction of high-density arrays.

During the fabrication of pressure sensor arrays, the crossing of conducting circuits was unnecessary since the electrodes were positioned perpendicular to the active sensing layers. However, the electrodes of strain sensors must be arranged on the same plane as the sensing elements. As the number of sensor units increased, the circuit crossing issues inevitably emerged. To address this issue, we employed a layered inkjet printing technique for the fabrication of sensor circuits. The entire fabrication process for the strain sensor array relied solely on inkjet printing. This technique incorporated an insulating isolation layer to ensure the insulation and division of the circuit, preventing the interference between horizontal and vertical circuit lines. Thus, three types of inks were used during this process: PEDOT:PSS conductive ink, silver nanoparticle conductive ink, and UV insulation ink. These inks functioned as the sensing elements, conductive circuits, and the insulation layers, respectively. The printing process encompassed four steps: printing horizontal silver conductive lines, printing the insulation layers, printing vertical silver conductive lines, and printing PEDOT:PSS sensing units. Ultimately, as

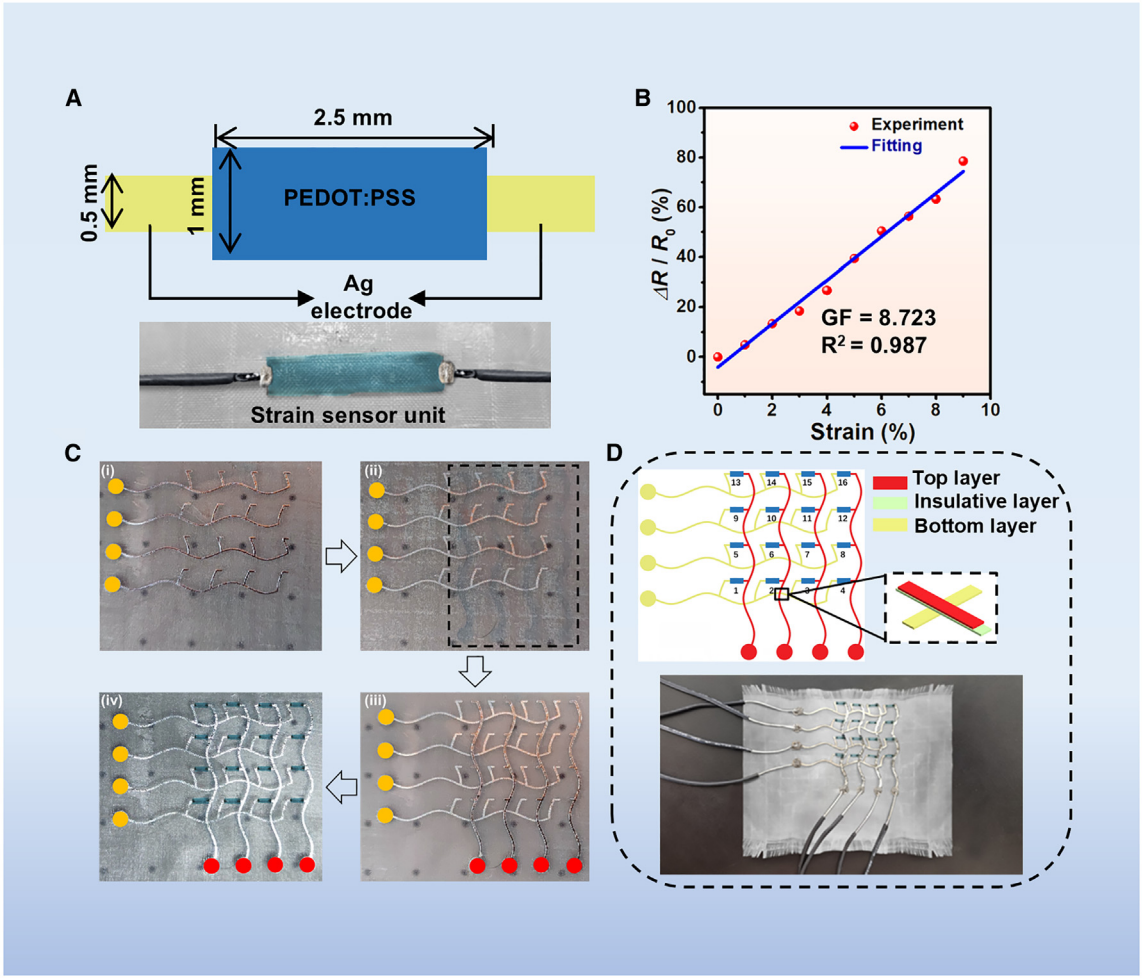

Figure 3. Schematic diagrams of the design and fabrication of strain sensor unit and array

(A) Schematic diagram of the strain sensor unit (top) and the photo of the inkjet-printed sensor unit (bottom).

(B) Relative resistance change (ΔR / R_0) of the sensor unit versus the applied strain of 1–9%.

(C) Photos of the inkjet printing process for a 4 × 4 strain sensor array.

(D) Schematic diagram of the strain sensor array (top) and the photo of the strain sensor array (bottom).

shown in Figure 3D, the sensor array featured a 4 × 4 array layout with a row and column spacing of 6.67 mm each. The effective measurement area of the sensor array was 4 cm^2, and the arrangement density was 4 units·cm^{-2}. This design and fabrication method enabled *in-situ* manufacturing of the flexible sensor array on the canopy fabric for the parachute strain measurement. The STAR Methods section provided a detailed description of the manufacturing processes and conditions.

Quality analysis of *in-situ* manufactured strain sensor array

As shown in Figures S6A and S6B, we selected one solder pad and one corner of the silver circuits as representative areas to evaluate the inkjet printing quality of the bottom conductive circuits. The printed solder pad displayed a regular shape with well-defined edges and the corners of the silver wire also displayed clear boundaries. Therefore, these results indicated inkjet printing process was successful for the bottom layer's silver circuits. Discontinuous cracks observed on the solder pads may be attributed to temperature fluctuations occurring during the fabrication process, specifically during the transition from a high-temperature curing environment to room temperature. However, it had a subtle impact on the conductivity of bottom silver circuits. The intersection points and corners of the silver circuit were selected as representative areas to evaluate the inkjet printing quality of the insulation layer and the top layer's circuits. As shown in Figures S6C and S6D, the insulation layer had regular edges and formed a bridging structure with the bottom layer's lines, ensuring effective insulation between the top and bottom layers. Additionally, the smoothness of the insulation layer ensured the surface of the upper silver circuit also remained smooth. Compared with the top silver circuits, the bottom silver circuits were uneven. This was because the parachute canopy fabric was less smooth than the insulation layer. Overall, the

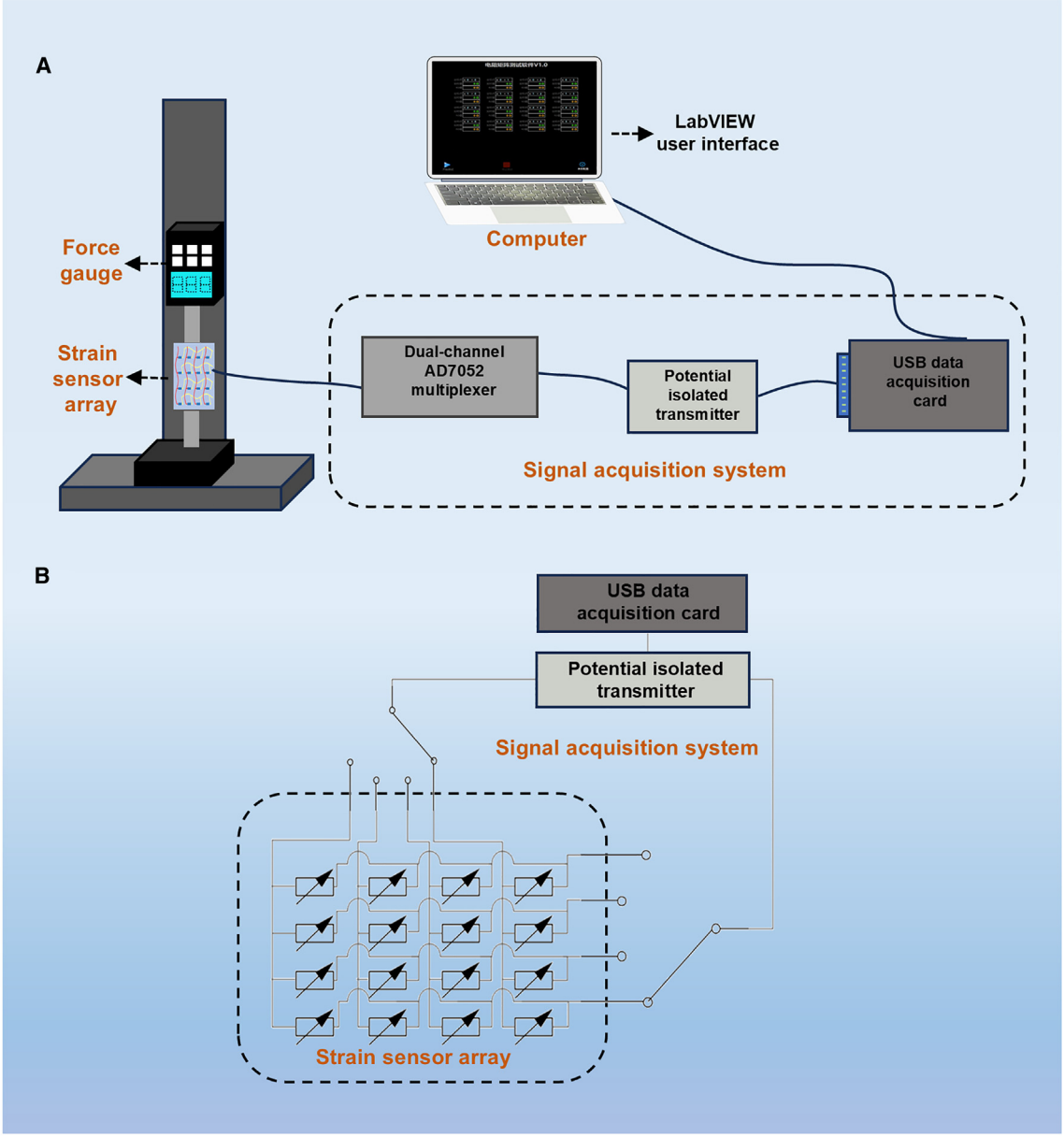

Figure 4. Schematic diagrams of the test setup and data acquisition design

(A) Schematic diagram of the test setup for evaluating strain sensor performance.

(B) Schematic diagram of the circuit structure for the strain sensor array and signal acquisition system.

inkjet printing quality met the requirements of the parachute strain measurement.

Mechanical and electrical characterization of the strain sensor array

As shown in Figure 4, the experimental setup for testing the properties of the strain sensor array included a tension testing machine and a data acquisition module. The data acquisition system composed of a multiplexer, an isolation transmitter, and a data acquisition card. A scanning circuit was used to measure the performance of each sensing unit. As shown in Figures 4A and S7, the voltage signals were collected by the data acquisition system and recorded via the LabVIEW user interface. And the interface showed the strain sensor array with 16 sensing units as follows: 1-(X_0, Y_0), 2-(X_0, Y_1), 3-(X_0, Y_2), 4-(X_0, Y_3); 5-(X_1, Y_0), 6-(X_1, Y_1), 7-(X_1, Y_2), 8-(X_1, Y_3); 9-(X_2, Y_0), 10-(X_2, Y_1), 11-(X_2, Y_2), 12-(X_2, Y_3); 13-(X_3, Y_0), 14-(X_3, Y_1), 15-(X_3, Y_2), and 16-(X_3, Y_3). Therefore, as shown in Figures 4B and S8, the scanning function of the circuits was achieved by controlling two AD7502 multiplexers with the data acquisition card. Two AD7502 multiplexers controlled the horizontal and vertical lines, alternately switching the signal paths on both sides to achieve

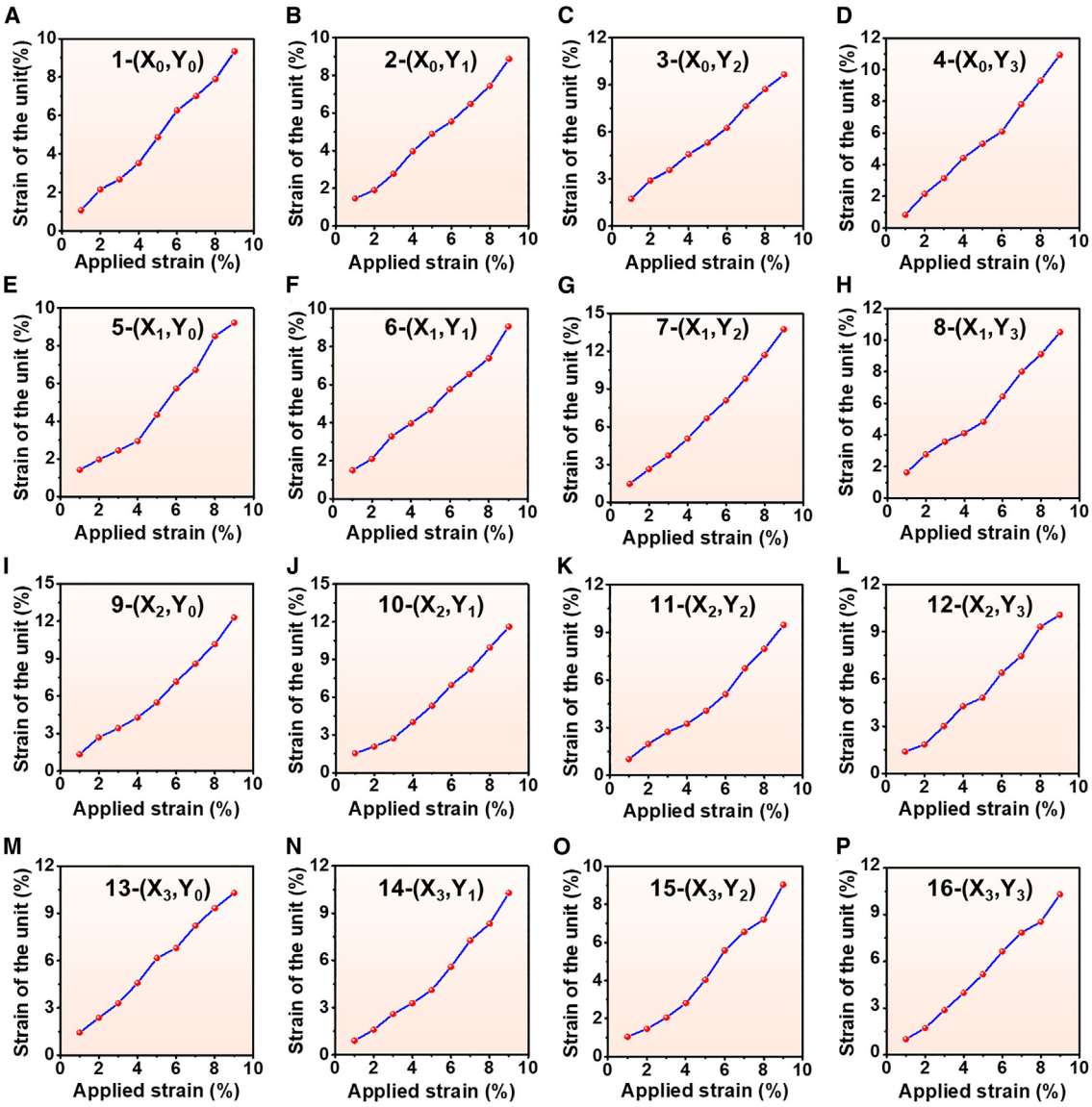

Figure 5. Strain variation curves for the 16 sensor units at coordinates

(A) 1-(X_0, Y_0), (B) 2-(X_0, Y_1), (C) 3-(X_0, Y_2), (D) 4-(X_0, Y_3), (E) 5-(X_1, Y_0), (F) 6-(X_1, Y_1), (G) 7-(X_1, Y_2), (H) 8-(X_1, Y_3); (I) 9-(X_2, Y_0), (J) 10-(X_2, Y_1), (K) 11-(X_2, Y_2), (L) 12-(X_2, Y_3), (M) 13-(X_3, Y_0), (N) 14-(X_3, Y_1), (O) 15-(X_3, Y_2), and (P) 16-(X_3, Y_3) as the entire fabric is stretched uniaxially

traversal measurements across the entire sensor array. The multiplexer had a data processing capability of 500 Hz and can convert resistance signals in the range of 0–50 kΩ into voltage signals in the range of 0–10 V. After the multiplexer selected a scanning node, the end of the PEDOT:PSS was connected to the isolation transmitter for signal conversion.

As shown in Figure S7B, we fixed the parachute canopy fabric with strain sensor array in the clamps of the tensile testing machine. The data acquisition card was connected to the Personal Computer (PC) and initiated the array scanning of the sensor resistances. The testing machine was set to a speed of 100 mm min^{-1} for applying strain to the fabric. The $\Delta R / R_0$ values for each sensor unit at applied fabric strain levels of 1%, 2%, 3%, 4%, 5%, 6%, 7%, and 9%, were input into the calibration equation depicted in Figure 3B. This enabled us to determine the strain corresponding for each sensing unit at different strain levels of entire canopy fabric. Figure 5 illustrated the curves of the relative resistance change ($\Delta R / R_0$) of each unit versus the applied strain on the fabric. The curves revealed that under uniaxial tension, strain values exhibited significant differences among different sensor units, demonstrating the sensor array's capability to measure the non-uniform strains in the fabric under deformation.

To clearly observe the non-uniform strain distribution in the testing area of canopy fabric, strain distribution maps were compiled under uniaxial stretching at strain levels of 1%, 2%, 3%, 4%, 5%, 6%, 7%, and 9%, respectively. As shown in

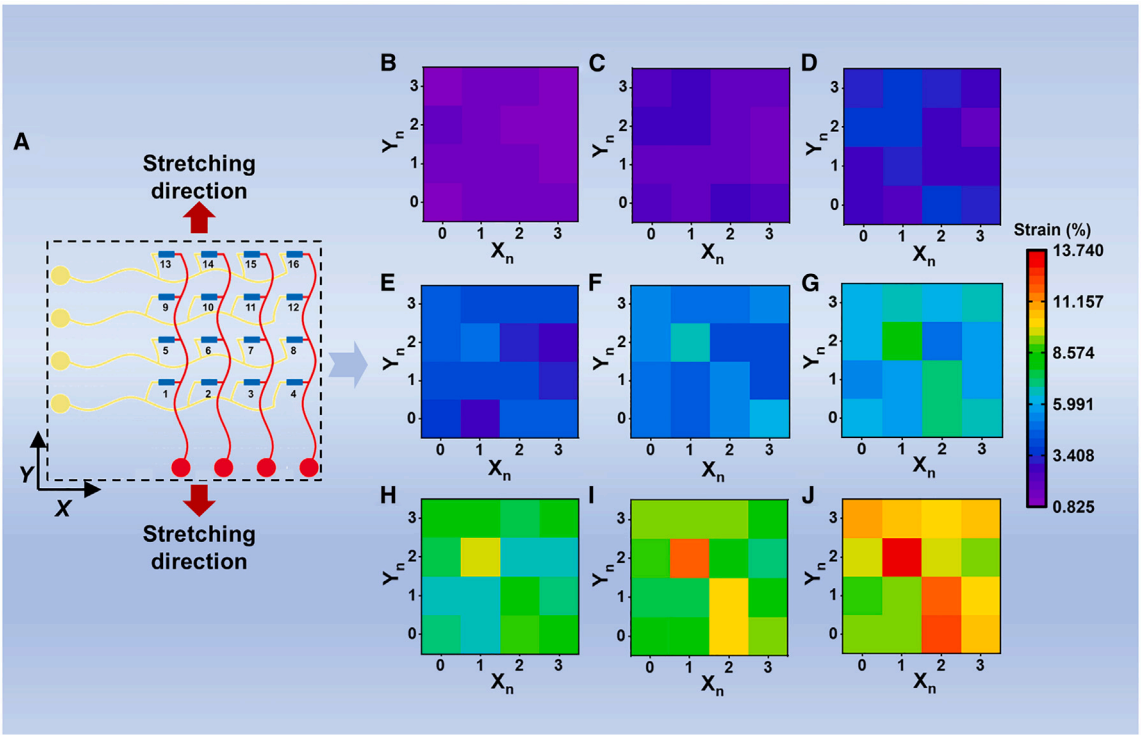

Figure 6. The strain distribution of the canopy fabric under stretching

(A) Schematic illustration of the canopy fabric with a sensor array under stretching.

(B-J) Strain distribution maps for the 16 sensor units of the strain sensor array at fabric strain values of (B) 1%, (C) 2%, (D) 3%, (E) 4%, (F) 5%, (G) 6%, (H) 7%, (I) 8%, and (J) 9%.

Figure 6, these maps clearly represented the distribution of strain magnitude during stretching. When the fabric strain exceeded 3%, as illustrated in Figures 6E–6J, the sensing unit 10-(X_2, Y_1) exhibited the highest strain value and was the first to fail. Consequently, these results collectively demonstrated that strain sensor array was effective in monitoring the strain distribution of the parachute canopy fabric during operation.

Conclusions

In summary, we proposed an effective method for fabricating a high-density sensor array on the parachute canopy fabric through inkjet printing, enabling the monitoring of non-uniform strains and strain magnitude distributions of the canopy fabric during deformation. By mimicking the outer waxy layer of coconut shells and using low-cost MS to treat the fabric surface, we successfully overcome capillary effects and optimized the substrate's wettability, thereby facilitating *in situ* inkjet printing of the sensor array on the parachute fabric. The printed sensor unit demonstrated good sensitivity and linearity. Then, the resulting sensor array was successfully fabricated using inkjet printing combined with a layered printing strategy. The approach not only simplified the circuit layout but also effectively addressed the issue of circuit crossing within the strain sensor array, allowing for an efficient spatial arrangement of sensor units. The high-density sensor array was integrated with a scanning circuit and data acquisition system to collect electrical signals from the array. Through tensile testing of the canopy fabric, the sensor array successfully monitored the relative resistance-strain curves of each sensing unit and non-uniform strain distribution in the stretched parachute canopy fabric. This research offered a viable method for the precise *in-situ* measurement of parachute fabric strains, contributing to the optimization of parachute structure design for aerospace applications.

Limitations of the study

We have presented a method for *in-situ* inkjet printing of the high-density strain arrays on bionically modified parachute fabric, successfully enabling the monitoring of non-uniform strains in the fabric. However, several issues remain unresolved in this study. First, although stable inkjet printing was successfully achieved on bionically modified parachute fabric using MS, a more in-depth investigation and explanation of the underlying wetting mechanisms were not conducted. Second, this study only demonstrated that the strain sensor array can monitor non-uniform strains of the parachute fabric under simple deformations. However, the sensing performance and signal decoupling under more complex deformations require further investigation. Addressing these issues will be the subjects of our future research.

RESOURCE AVAILABILITY

Lead contact

Further information and requests for resources and reagents should be directed to and will be fulfilled by the lead contact, Dengbao Xiao (xiaodengbao@bit.edu.cn).

Materials availability

This study did not generate new unique reagents.

Data and code availability

- All data reported in this paper will be shared by the lead contact upon request.
- This paper does not report original code.
- Any additional information required to reanalyze the data reported in this paper is available from the lead contact upon request.

ACKNOWLEDGMENTS

This work was supported by the National Key R&D Program of China (2023YFB3309100 and 2024YFB3310300) and the National Natural Science Foundation of China (grant no. 12172055).

AUTHOR CONTRIBUTIONS

H.L. and J.H. contributed equally to the article. H.L., writing – original draft, methodology, investigation, visualization, conceptualization. J.H., writing – original draft, investigation, conceptualization. C.L., resources, formal analysis, project administration. F.B., data curation, investigation. X.L., investigation, visualization. X.W., visualization. Z.W., visualization. X.B., visualization. D.X., writing – review & editing, supervision, investigation, funding acquisition, conceptualization. H.J., resources, writing – review & editing, supervision, conceptualization. W.R., writing – review & editing, supervision.

DECLARATION OF INTERESTS

The authors declare no competing interests.

STAR★METHODS

Detailed methods are provided in the online version of this paper and include the following:

- KEY RESOURCES TABLE
- METHOD DETAILS
  - Surface modification of the canopy fabric
  - Characterization of the water contact angle
  - Design and fabrication of strain sensing units
  - Construction of the strain sensor array based on Parachute canopy fabric
  - Other characterizations
  - Finite element Analyses of deformation
- QUANTIFICATION AND STATISTICAL ANALYSIS

SUPPLEMENTAL INFORMATION

Supplemental information can be found online at https://doi.org/10.1016/j.isci.2025.111794.

Received: November 4, 2024
Revised: December 16, 2024
Accepted: January 9, 2025
Published: January 13, 2025

REFERENCES

1. Xue, X., and Wen, C.-Y. (2021). Review of unsteady aerodynamics of supersonic parachutes. Prog. Aeronaut. Sci. *125*, 100728. https://doi.org/10.1016/j.paerosci.2021.100728.
2. Gonyea, K.C., Tanner, C.L., Clark, I.G., Kushner, L.K., Schairer, E.T., and Braun, R. (2013). Aerodynamic stability and performance of next-generation parachutes for mars entry, descent, and landing. In AIAA Aerodynamic Decelerator Systems (ADS) Conference. https://doi.org/10.2514/6.2013-1356.
3. Li, Y., Qu, C., Li, J., and Yu, L. (2023). Modelling of parachute airborne clusters flight dynamics and parachute interactions. Aerospace *10*, 51. https://doi.org/10.3390/aerospace10010051.
4. Favini, E., Niezrecki, C., Manohar, S.K., Willis, D., Chen, J., Niemi, E., Desabrais, K., and Charette, C. (2011). Sensing performance of electrically conductive fabrics and dielectric electro active polymers for parachutes. In Sensors and Smart Structures Technologies for Civil, Mechanical, and Aerospace Systems. https://doi.org/10.1177/1045389X12453959.
5. Li, M., Pei, Y., Cao, Y., Chen, S., and Guo, X. (2021). Flexible strain sensors: from devices to array integration. Flex. Print. Electron. *6*, 043002. https://doi.org/10.1088/2058-8585/ac20bf.
6. Pang, C., Lee, G.-Y., Kim, T.i., Kim, S.M., Kim, H.N., Ahn, S.-H., and Suh, K.-Y. (2012). A flexible and highly sensitive strain-gauge sensor using reversible interlocking of nanofibres. Nat. Mater. *11*, 795–801. https://doi.org/10.1038/nmat3380.
7. Wang, S., Gong, L., Shang, Z., Ding, L., Yin, G., Jiang, W., Gong, X., and Xuan, S. (2018). Novel safeguarding tactile e-skins for monitoring human motion based on SST/PDMS-AgNW-PET hybrid structures. Adv. Funct. Mater. *28*, 1707538. https://doi.org/10.1002/adfm.201707538.
8. Kim, K.K., Hong, S., Cho, H.M., Lee, J., Suh, Y.D., Ham, J., and Ko, S.H. (2015). Highly sensitive and stretchable multidimensional strain sensor with prestrained anisotropic metal nanowire percolation networks. Nano Lett. *15*, 5240–5247. https://doi.org/10.1021/acs.nanolett.5b01505.
9. Li, S., Liu, G., Li, R., Li, Q., Zhao, Y., Huang, M., Zhang, M., Yin, S., Zhou, Y., Tang, H., et al. (2022). Contact-resistance-free stretchable strain sensors with high repeatability and linearity. ACS Nano *16*, 541–553. https://doi.org/10.1021/acsnano.1c07645.
10. Mendoza, S., Mendoza, E., Prohaska, J., Antreas, T., Esterkin, Y., Theodosiou, A., Kalli, K., Kelsay, C., Lowry, C., Hill, P., et al. (2023). Dynamics of smart parachute airborne deployment using broadcloth canopy instrumented with an array of weaved distributed fiber optic strain sensors. In European Workshop on Structural Health Monitoring, pp. 88–96. https://doi.org/10.1007/978-3-031-07258-1_10.
11. Favini, E., Agnihotra, S., Surwade, S.P., Niezrecki, C., Willis, D., Chen, J., Niemi, E., Desabrais, K., Charette, C., and Manohar, S.K. (2012). Sensing performance of electrically conductive fabrics and suspension lines for parachute systems. J. Intell. Mater. Syst. Struct. *23*, 1969–1986. https://doi.org/10.1177/1045389x12453959.
12. Budolak, D.W., Hantsche, L.J., and Fuente, E.R.D.L. (2022). Strain sensor survey for parachute canopy load measurements. In 26th AIAA Aerodynamic Decelerator Systems Technology Conference. https://doi.org/10.2514/6.2022-2754.
13. Cochrane, C., Lewandowski, M., and Koncar, V. (2010). A flexible strain sensor based on a conductive polymer composite for *in situ* measurement of parachute canopy deformation. Sensors *10*, 8291–8303. https://doi.org/10.3390/s100908291.
14. Khalid, M.A.U., and Chang, S.H. (2022). Flexible strain sensors for wearable applications fabricated using novel functional nanocomposites: A review. Compos. Struct. *284*, 115214. https://doi.org/10.1016/j.compstruct.2022.115214.
15. Wang, J., Xue, P., Tao, X., and Yu, T. (2013). Strain sensing behavior and its mechanisms of electrically conductive PPy-coated fabric. Adv. Eng. Mater. *16*, 565–570. https://doi.org/10.1002/adem.201300407.
16. Wang, J., Lu, C., and Zhang, K. (2019). Textile-based strain sensor for human motion detection. Energy Environ. Mater. *3*, 80–100. https://doi.org/10.1002/eem2.12041.
17. Carney, A., Niezrecki, C., Niemi, E.E., Jr., and Chen, J. (2007). Parachute strain and deformation measurements using imaging and polymer strain sensors. In 19th AIAA Aerodynamic Decelerator Systems Technology Conference and Seminar. https://doi.org/10.2514/6.2007-2553.

18. Bazin, J., Tutt, B., Mendoza, E., Hill, P., Willey, N., and Crane, R. (2019). Feasibility of Weaved Distributed Fiber Optic Sensors in Parachute Broadcloth for Strain Measurement. In AIAA Aviation 2019 Forum. https://doi.org/10.2514/6.2019-2891.

19. Rabinovitch, J., Griffin, G.S., Seto, W., O'Farrell, C., Tanner, C.L., and Clark, I.G. (2020). Full-scale supersonic parachute shape reconstruction using three-dimensional stereo imagery. J. Spacecr. Rockets *57*, 1139–1152. https://doi.org/10.2514/1.A34717.

20. Jo, J., Xu, A., Mishra, A.K., Bai, H., Derkevorkian, A., Rabinovitch, J., Park, H., and Shepherd, R.F. (2022). Measurement of parachute canopy textile deformation using mechanically invisible stretchable lightguides. Adv. Mater. Technol. *7*, 2200437. https://doi.org/10.1002/admt.202200437.

21. Seyedin, S., Zhang, P., Naebe, M., Qin, S., Chen, J., Wang, X., and Razal, J.M. (2019). Textile strain sensors: a review of the fabrication technologies, performance evaluation and applications. Mater. Horiz. *6*, 219–249. https://doi.org/10.1039/c8mh01062e.

22. Zhang, J.-W., Zhang, Y., Li, Y.-Y., and Wang, P. (2021). Textile strain sensors: a review of the fabrication technologies, performance evaluation and applications. Polym. Rev. *62*, 65–94. https://doi.org/10.1080/15583724.2021.1901737.

23. Madhavan, R. (2022). Flexible and stretchable strain sensors fabricated by inkjet printing of silver nanowire-ecoflex composites. J. Mater. Sci. Mater. Electron. *33*, 3465–3484. https://doi.org/10.1007/s10854-021-07540-8.

24. Karim, M.A.U., Chung, S., Alon, E., and Subramanian, V. (2016). Fully inkjet-printed stress-tolerant microelectromechanical reed relays for large-area electronics. Adv. Electron. Mater. *2*, 1500482. https://doi.org/10.1002/aelm.201500482.

25. Finn, D.J., Lotya, M., and Coleman, J.N. (2015). Inkjet printing of silver nanowire networks. ACS Appl. Mater. Interfaces *7*, 9254–9261. https://doi.org/10.1021/acsami.5b01875.

26. Lemarchand, J., Bridonneau, N., Battaglini, N., Carn, F., Mattana, G., Piro, B., Zrig, S., and Noël, V. (2022). Challenges, prospects, and emerging applications of inkjet-printed electronics: a chemist's point of view. Angew. Chem. Int. Ed. *61*, e202200166. https://doi.org/10.1002/anie.202200166.

27. Arya, P., Wu, Y., Wang, F., Wang, Z., Cadilha Marques, G., Levkin, P.A., Nestler, B., and Aghassi-Hagmann, J. (2024). Wetting behavior of inkjet-printed electronic inks on patterned substrates. Langmuir *40*, 5162–5173. https://doi.org/10.1021/acs.langmuir.3c03297.

28. Al-Halhouli, A., Qitouqa, H., Alashqar, A., and Abu-Khalaf, J. (2018). Inkjet printing for the fabrication of flexible/stretchable wearable electronic devices and sensors. Sens. Rev. *38*, 438–452. https://doi.org/10.1108/sr-07-2017-0126.

29. Shahariar, H., Kim, I., Soewardiman, H., and Jur, J.S. (2019). Inkjet printing of reactive silver ink on textiles. ACS Appl. Mater. Interfaces *11*, 6208–6216. https://doi.org/10.1021/acsami.8b18231.

30. Liang, Y., Liu, X., Fang, K., An, F., Li, C., Liu, H., Qiao, X., and Zhang, S. (2021). Construction of new surface on linen fabric by hydroxyethyl cellulose for improving inkjet printing performance of reactive dyes. Prog. Org. Coat. *154*, 106179. https://doi.org/10.1016/j.porgcoat.2021.106179.

31. Hajipour, A., and Nateri, S.A. (2018). The effect of weave structure on the quality of inkjet polyester printing. J. Text. Inst. *110*, 799–806. https://doi.org/10.1080/00405000.2018.1529722.

32. Li, M., Zhang, L., An, Y., Ma, W., and Fu, S. (2018). Relationship between silk fabric pretreatment, droplet spreading, and ink-jet printing accuracy of reactive dye inks. J. Appl. Polym. Sci. *135*, 46703. https://doi.org/10.1002/app.46703.

33. Teixidó, H., Staal, J., Caglar, B., and Michaud, V. (2022). Capillary effects in fiber reinforced polymer composite processing: a review. Front. Mater. *9*, 809226. https://doi.org/10.3389/fmats.2022.809226.

34. Li, M., Li, C., Blackman, B.R., and Eduardo, S. (2021). Mimicking nature to control bio-material surface wetting and adhesion. Int. Mater. Rev. *67*, 658–681. https://doi.org/10.1080/09506608.2021.1995112.

35. Xue, D., Zhang, X., Lu, X., Chen, G., and Chen, Z.-H. (2017). Molecular and evolutionary mechanisms of cuticular wax for plant drought tolerance. Front. Plant Sci. *8*, 621. https://doi.org/10.3389/fpls.2017.00621.

36. Jetter, R., and Sodhi, R. (2011). Chemical composition and microstructure of waxy plant surfaces: triterpenoids and fatty acid derivatives on leaves of Kalanchoe daigremontiana. Sur. Interface Anal. *43*, 326–330. https://doi.org/10.1002/sia.3430.

37. Koch, K., Bhushan, B., and Barthlott, W. (2008). Diversity of structure, morphology and wetting of plant surfaces. Soft Matter *4*, 1943–1963. https://doi.org/10.1039/b804854a.

38. Guan, H., Han, Z., Cao, H., Niu, S., Qian, Z., Ye, J., and Ren, L. (2015). Characterization of multi-scale morphology and superhydrophobicity of water bamboo leaves and biomimetic polydimethylsiloxane (PDMS) replicas. J. Bionic Eng. *12*, 624–633. https://doi.org/10.1016/s1672-6529(14)60152-9.

39. Zhang, W., Lu, P., Qian, L., and Xiao, H. (2014). Fabrication of superhydrophobic paper surface via wax mixture coating. Chem. Eng. J. *250*, 431–436. https://doi.org/10.1016/j.cej.2014.04.050.

40. Yan, M., Liu, W., Lan, X., Li, T., and Zhao, W. (2023). W. Multi-stimulus response behavior of biomimetic autocrine waxy materials for potential self-constructing surface microstructures. ACS Appl. Mater. Interfaces *15*, 47822–47832. https://doi.org/10.1021/acsami.3c11357.

41. Yi, M., Wu, L., Liu, L., Zhang, P., and Li, X. (2020). Research on the typical microstructures and contact angles of hydrophobic plant leaves. Micro & Nano Lett. *15*, 250–254. https://doi.org/10.1049/mnl.2019.0323.

42. Wang, F., and Nestler, B. (2024). Wetting and contact-angle hysteresis: density asymmetry and van der waals force. Phys. Rev. Lett. *132*, 126202. https://doi.org/10.1103/PhysRevLett.132.126202.

43. Fan, X., Nie, W., Tsai, H., Wang, N., Huang, H., Cheng, Y., Wen, R., Ma, L., Yan, F., and Xia, Y. (2019). PEDOT:PSS for flexible and stretchable electronics: modifications, strategies, and applications. Adv. Sci. *6*, 1900813. https://doi.org/10.1002/advs.201900813.

44. Wen, Y., and Xu, J. (2017). Scientific importance of water-processable PEDOT-PSS and preparation, challenge and new application in sensors of its film electrode: a review. J. Polym. Sci., Part A: Polym. Chem. *55*, 1121–1150. https://doi.org/10.1002/pola.28482.

45. Wang, G., Tao, X., and Wang, R. (2008). Fabrication and characterization of OLEDs using PEDOT:PSS and MWCNT nanocomposites. Compos. Sci. Technol. *68*, 2837–2841. https://doi.org/10.1016/j.compscitech.2007.11.004.

46. Sun, F., Liu, L., Liu, T., Wang, X., Qi, Q., Hang, Z., Chen, K., Xu, J., and Fu, J. (2023). Vascular smooth muscle-inspired architecture enables soft yet tough self-healing materials for durable capacitive strain-sensor. Nat. Commun. *14*, 130. https://doi.org/10.1038/s41467-023-35810-y.

47. Yu, P., Qi, L., Guo, Z., Lin, S., Liu, Y., and Zhao, J. (2022). Arbitrary-shape-adaptable strain sensor array with optimized circuit layout via direct-ink-writing: Scalable design and hierarchical printing. Mater. Des. *214*, 110388. https://doi.org/10.1016/j.matdes.2022.110388.

STAR★METHODS

KEY RESOURCES TABLE

REAGENT or RESOURCE	SOURCE	IDENTIFIER
Chemicals, peptides, and recombinant proteins		
Aerospace parachute canopy fabric	China Academy of Space Technology	N/A
Modified silane	Chengdu Guibao Technology Co., Ltd.	GUIBAO 603MS
Conductive silver nanoparticle ink	Beijing BroadTeko Co., Ltd.	BroadCON INK550
PEDOT:PSS conductive ink	Beijing BroadTeko Co., Ltd.	BroadCON-PTS1000
Conductive silver adhesive	Zhuhai Kingsname Technology Co. Ltd.	K-818
Polydimethylsiloxane matrix	Dow Corning Co., Ltd.	Sylgard 184
Curing agent	Dow Corning Co., Ltd.	Sylgard 184
Software and algorithms		
Abaqus	Dassault Systèmes	https://www.3ds.com/products/simulia/abaqus
Other		
Digital inkjet printer	Beijing BroadTeko Co., Ltd.	FA0302
Contact angle meter	Shanghai Sunzerm Instrument Co., Ltd.	SZ-CAMC32
Drying oven	Shaoxing Sobo Co., Ltd.	101-1
Vacuum drying oven	Shanghai Yiheng Scientific Instrument Co., Ltd.	DZF-6096
Potentiometer transmitter isolator	Guanhangda Co., Ltd.	KB1-60
Data acquisition card	ART Tech Co., Ltd.	USB3200N
Multiplexer	Analog Devices, Inc.	AD7502
LCR meter	Shenzhen Yisheng Shengli Technology Co., Ltd.	VC4090A
Tensile testing machine	Wenzhou Weidu Electronics Co., Ltd.	SJX-S-400-1000 N
Scanning electron microscopy	Hitachi Co., Ltd.	HITACHISU5000
Optical microscope	Shenzhen Aosvi Optical Instrument Co., Ltd.	A0-4K32C

METHOD DETAILS

Surface modification of the canopy fabric

The parachute canopy fabric was smoothly and securely affixed to a glass plate using double-sided tape. An appropriate amount of MS was applied to the fabric with a glue gun, and then the adhesive was evenly spread over the fabric using a spatula. The coated canopy fabric was cured in a convection oven at 60°C for 1 h. Then the modified canopy fabric was fabricated.

Characterization of the water contact angle

The static water contact angles of semiaquilegia adoxoide, lagedium sibiricum, coconut shell and modified canopy fabric were characterized on the contact angle instrument (SZ-CAMC32,Shanghai Sunzerm Instrument Co., Ltd., China) using 3 μL water droplets.

Design and fabrication of strain sensing units

The PEDOT:PSS sensing layer and silver electrode were printed on the rectangular modified canopy fabric using a digital inkjet printer (FA0302, Beijing BroadTeko Co., Ltd., China). Then the conductive silver paste was used to bond the silver electrodes to copper wires. After curing the conductive silver paste at 80°C for 30 min, the fabrication of the strain sensing units was finally completed.

Construction of the strain sensor array based on Parachute canopy fabric

The strain sensor array was fabricated by using a digital inkjet printer. The glass substrate with the modified canopy fabric, as prepared in the *Section "*surface modification of the canopy fabric*"*, was moved to the printing stage. Its positional coordinates were recorded to ensure a consistent reference baseline for each printing step. The printing patterns for each step were designed in AutoCAD and then were converted to TIFF bitmap format using Photoshop for importing into the printer.

First, as shown in Figure 3C i, the horizontal silver circuits on the bottom layer were printed using conductive silver nanoparticle ink. The inkjet printer's printing mode was set at high ink volume mode with the printing frequency of 8 PASS. The nozzle height was set to 2 mm above the printing platform and then the printing process started. After finishing the printing process, the printed pattern was set in a drying oven (101-1, Shaoxing Sobo Co., Ltd., China) at 150°C for 30 min. In order to minimize the resistance of the printed circuit lines, it was necessary to increase the thickness of the printed lines by repetitive printing and curing. Multiple experiments have shown that when the number of repetitions was 15, the resistance of the silver circuit lines met requirement.

Second, as shown in Figure 3C ii, the insulation layer was printed using UV insulation ink. During the printing process, the UV LED was turned on. The insulation ink should be printed with a uniform thickness to prevent excessive height differences, which could lead to poor circuit contact. The printing frequency was set to 4 PASS, and the insulation isolation layer was finished after two repeated printing processes.

Third, as shown in Figure 3C iii, the process of inkjet printing of vertical silver circuits was similar to the horizontal silver circuits. The average resistance of the silver circuits was measured to be 50 Ω.

Fourth, as shown in Figure 3C iv, the strain sensor units were printed with PEDOT:PSS ink. To minimize the impact of silver circuit resistance, the resistance of PEDOT:PSS sensing unit needed to be within an appropriate range. After 5 rounds of inkjet printing and curing of the PEDOT:PSS sensing units, the initial average resistance of the sensing units was 3.2 kΩ. Therefore, the resistance of PEDOT:PSS ($R_{PEDOT:PSS}$) was significantly greater than that of silver (R_{Ag}), indicating that the PEDOT:PSS sensing units met the design requirements. The 8 wires of the data acquisition system were bonded with their corresponding solder pads using conductive silver paste, and subsequently cured in a drying oven to cure at 80°C for 30 min.

Finally, the strain sensor array was encapsulated. The polydimethylsiloxane (PDMS) and curing agent were thoroughly mixed in a weight ratio of 10:1, and the mixture was set in a vacuum drying oven (DZF-6096, Shanghai Yiheng Scientific Instrument Co., Ltd., China) for removing the air bubbles. Next, the PDMS mixture was applied over the cured silver circuits and sensing units, and then cured in an oven at 80°C for 2 h.

Other characterizations

The data acquisition module was consisted of a potentiometer transmitter isolator (KB1-60, Guanhangda Co., Ltd., China), a data acquisition card (USB3200N, ART Technology Co., Ltd., China) and a multiplexer (AD7502, Analog Devices, Inc., China). The resistance signals were measured by the LCR meter (VC4090A, Shenzhen Yisheng Shengli Technology Co., Ltd., China). The stretching tests were carried out by a tensile testing machine (SJX-S-400-1000 N, Wenzhou Weidu Electronics Co., Ltd., China). The scanning electron microscopy (SEM) images were taken by a field emission scanning electron microscope (HITACHISU5000, Hitachi Co., Ltd., Japan). The optical microscope images were taken by an optical microscope (A0-4K32C, Shenzhen Aosvi Optical Instrument Co., Ltd., China).

Finite element Analyses of deformation

The mechanical deformation and strain distribution of the parachute during uniaxial stretching, biaxial stretching, and dislocation processes were obtained through finite element analysis (FEA). FEA was performed employing the commercial software ABAQUS (SIMULIA, France). The material parameters of nylon 66 fibers, which was regarded as a hyperelastic material described by the Yeoh model, were C_{10} = 43.7422775, C_{20} = 431.368287, C_{30} = -1267.91706.

QUANTIFICATION AND STATISTICAL ANALYSIS

Figures shown in the text were produced by Origin 2021 and Microsoft PowerPoint 2021 from the raw data. The FEA simulation data was obtained using ABAQUS software.